PNAS RESEARCH ARTICLE | APPLIED BIOLOGICAL SCIENCES SUSTAINABILITY SCIENCE

Bioinspired stretchable molecular composites of 2D-layered materials and tandem repeat proteins

Mert Vural[a], Tarek Mazeed[a], Dong Li[b,c], Oguzhan Colak[a], Reginald F. Hamilton[a], Huajian Gao[b,c], and Melik C. Demirel[a,d,1]

Edited by Ivet Bahar, University of Pittsburgh School of Medicine, Pittsburgh, PA; received November 4, 2021; accepted April 20, 2022

Protein based composites, such as nacre and bone, show astounding evolutionary capabilities, including tunable physical properties. Inspired by natural composites, we studied assembly of atomistically thin inorganic sheets with genetically engineered polymeric proteins to achieve mechanically compliant and ultra-tough materials. Although bare inorganic nanosheets are brittle, we designed flexible composites with proteins, which are insensitive to flaws due to critical structural length scale (~2 nm). These proteins, inspired by squid ring teeth, adhere to inorganic sheets via secondary structures (i.e., β-sheets and α-helices), which is essential for producing high stretchability (59 ± 1% fracture strain) and toughness (54.8 ± 2 MJ/m^3). We find that the mechanical properties can be optimized by adjusting the protein molecular weight and tandem repetition. These exceptional mechanical responses greatly exceed the current state-of-the-art stretchability for layered composites by over a factor of three, demonstrating the promise of engineering materials with reconfigurable physical properties.

2D-layered materials | tandem repeat proteins | mechanical properties | biomimetics

Significance

Molecular composites are ubiquitous in nature (e.g., bone and nacre) that have important functions from self-defense to carbon sequestering. Various life forms on Earth sequester carbon (e.g., shell-building marine animals) by combining proteins and inorganic layered composites. These composites become insensitive to flaws as soon as the structural size reaches a critical length. We studied mechanical properties of atomistically thin inorganic layers with tandem repeat proteins through fine control of their molecular weight. Mechanical properties are tunable and exceed state state-of-the-art composites, which cannot be explained by an existing theoretical model. This finding opens a perspective on failure mechanism for composites, which depends on interfacial rather than bulk properties. Controlling interfacial strength ultimately engender new design rules for nature-inspired composites.

Protein materials endow biological systems with amazing capabilities, including tunable control of structural (1), optical (2), electrical (3), self-healing (4) and thermal properties (5). Similarly, protein-based composites show extraordinary physical properties, which employ an ordered composite structure to establish superior mechanical strength and toughness (6, 7). The length scale of the unit structure (e.g., aspect ratio and interlayer distance) in these composites is definitive for their mechanical properties (6, 7). If structural order in micro dimension is designed and translated into bulk materials, then composites could be manufactured with extraordinary mechanical properties (6, 7). To give an example, the structure of red abalone shells [a natural nacre (8, 9)] is made of an adhesive protein layer with a thickness around 100–150 nm placed in between 400–500 nm thick inorganic (aragonite), which offers a toughness of 1.8 MJ/m^3 and a fracture strength of 135 MPa (Fig. 1*A*). A structurally more refined natural composite like bone is composed of bundles of mineralized collagen fibrils (~100 nm in diameter) and mineral nanoplatelets (few nanometers thick) (Fig. 1*B*) (6, 7, 10, 11). For example, femoral bone can match the mechanical strength of nacre, while having a superior ability to deform (1.9% tensile fracture strain) (10, 12). To achieve materials exceeding toughness of natural composites, there has been a research effort to synthetically engineer nanocomposites (13, 14) Two-dimensional (2D)-layered material with atomic thickness is an excellent candidate for filler material in these composites (15–24). In addition, 2D materials exhibit extraordinary mechanical properties stemming from their nanocrystalline nature, which consist of single or few layered crystals (25–28). However, it is fundamentally difficult to manufacture composites with extraordinary mechanical properties due to random distribution of nanosheets in organic matrix resulting from large interlayer distances and poor interfacial interactions between nanosheets and organic matrix (15–17, 19, 21). These structural and compositional constraints lead to inefficient stress transfer in between mechanically strong nanosheets (29, 30). Employing proper organic matrix materials in structural composites that facilitate specific interactions with 2D crystals can help orchestrate distribution of 2D crystals and promote order in these composites (18, 20, 22–24, 30). In addition, these organic matrices can facilitate efficient transfer of load via the high shear zones between 2D sheets (31, 32). Physical and chemical bonding between organic matrix and 2D crystals [e.g., π–π interactions, ionic bonding (22, 30) or permanently crosslinking (18), or 2D heterostructured fillers (24, 33)] can improve mechanical strength of composites, but these material systems can hardly exceed a fracture strain of 15% (22, 24, 30). On the other hand, softer composite systems can reach higher fracture strains, but they exhibit significantly lower toughness values compared to crystalline composites (34–36).

Here, we present a bioengineered composite that can exhibit remarkable mechanical stretchability and toughness. In this work, we introduce a tandem repeat protein matrix

Author contributions: M.C.D. designed research; M.V., T.M., D.L., and O.C. performed research; D.L., R.F.H., and H.G. contributed new reagents/analytic tools; M.V., T.M., D.L., O.C., R.F.H., H.G., and M.C.D. analyzed data; and M.V. and M.C.D. wrote the paper.

Competing interest statement: The authors declare that authors have issued and pending patents.

This article is a PNAS Direct Submission.

Copyright © 2022 the Author(s). Published by PNAS. This article is distributed under Creative Commons Attribution-NonCommercial-NoDerivatives License 4.0 (CC BY-NC-ND).

[1]To whom correspondence may be addressed. Email: mdemirel@engr.psu.edu.

This article contains supporting information online at http://www.pnas.org/lookup/suppl/doi:10.1073/pnas.2120021119/-/DCSupplemental.

Published July 26, 2022.

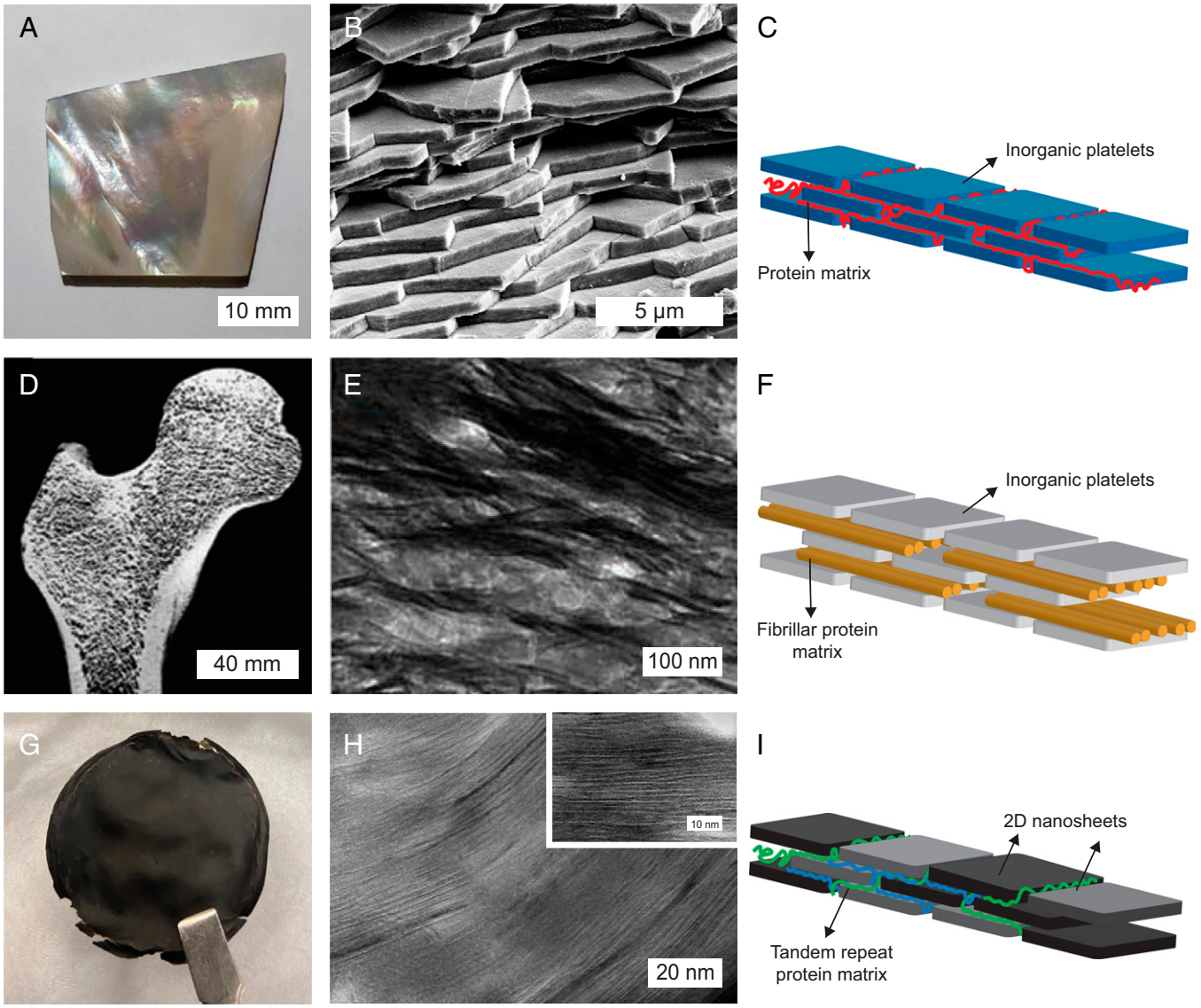

Fig. 1. (*A*) Optical image, (*B*) SEM cross-section, and (*C*) schematic of red abalone shells, highlighting their composite structure consisting of μm scale inorganic platelets and soft protein matrix. (*D*) SEM image (10), (*E*) TEM image (11), and (*F*) schematic of femoral bone, reflecting its composite nature composed of 100 nm long, several nanometers thick inorganic platelets supported by fibrillar collagen matrix (bone images reproduced with permission from ref. 10) (10, 11). (*G*) Optical image, (*H*) TEM image (*Inset*, higher resolution), and (*I*) schematic for bioengineered composites of tandem repeat proteins and 2D nanosheets, which exhibit an order in the scale of nanometers.

inspired from squid ring teeth proteins, which can form physical interactions with several nanosheets including graphene oxide (GO) and $Ti_3C_2T_x$ (MXene) (Fig. 1*C*). These interactions facilitate formation of an ordered structure, which consists of alternating layers of nanosheet and proteins. This hierarchical bilayer structure is confined into a length scale of 2 nm (Fig. 1*C*), which can be altered with angstrom level precision by tuning the number of tandem repeats (i.e., the molecular weight of proteins). These structural and compositional contributions are key for establishing deformation mechanisms that enables enhanced fracture strain values reaching 59 ± 1% without compromising material strength. Along with these qualities, we demonstrated that employing GO, MXene, and proteins in a single composite leads to sustainable composites with an outstanding toughness value of 54.8 ± 2 MJ/m^3, which, to the best of our knowledge, exceeds existing layered composites assembled from 2D crystals.

Self-Assembly of Bioengineered Composites

We utilized graphene oxide (GO) and $Ti_3C_2T_x$ (MXene) nanocrystals as filler materials to match tandem repeat protein-based matrix, since each component is proficient at hydrogen bond formation (Fig. 2*A*). Hydrogen bonding is also detrimental for the self-assembly kinetics of engineered tandem repeat (TR) proteins (1, 37). The amino acid sequence of engineered tandem repeat proteins are based on crystal-forming (AAASVSTVHHP) and amorphous (YGYGGLYGGLYGGLGYGP) sections of the amino acid sequence inspired from squid ring teeth of *Loligo vulgaris* (Fig. 2*A*) (1). These sequences are key elements for the assembly of secondary structures in these bioengineered proteins, as recently demonstrated by solid state nuclear magnetic resonance (NMR) experiments (37). In particular, β-sheet formations in TR proteins resemble 2D nanosheets, which are proven to be effective templates for 2D materials with hydrogen bonding

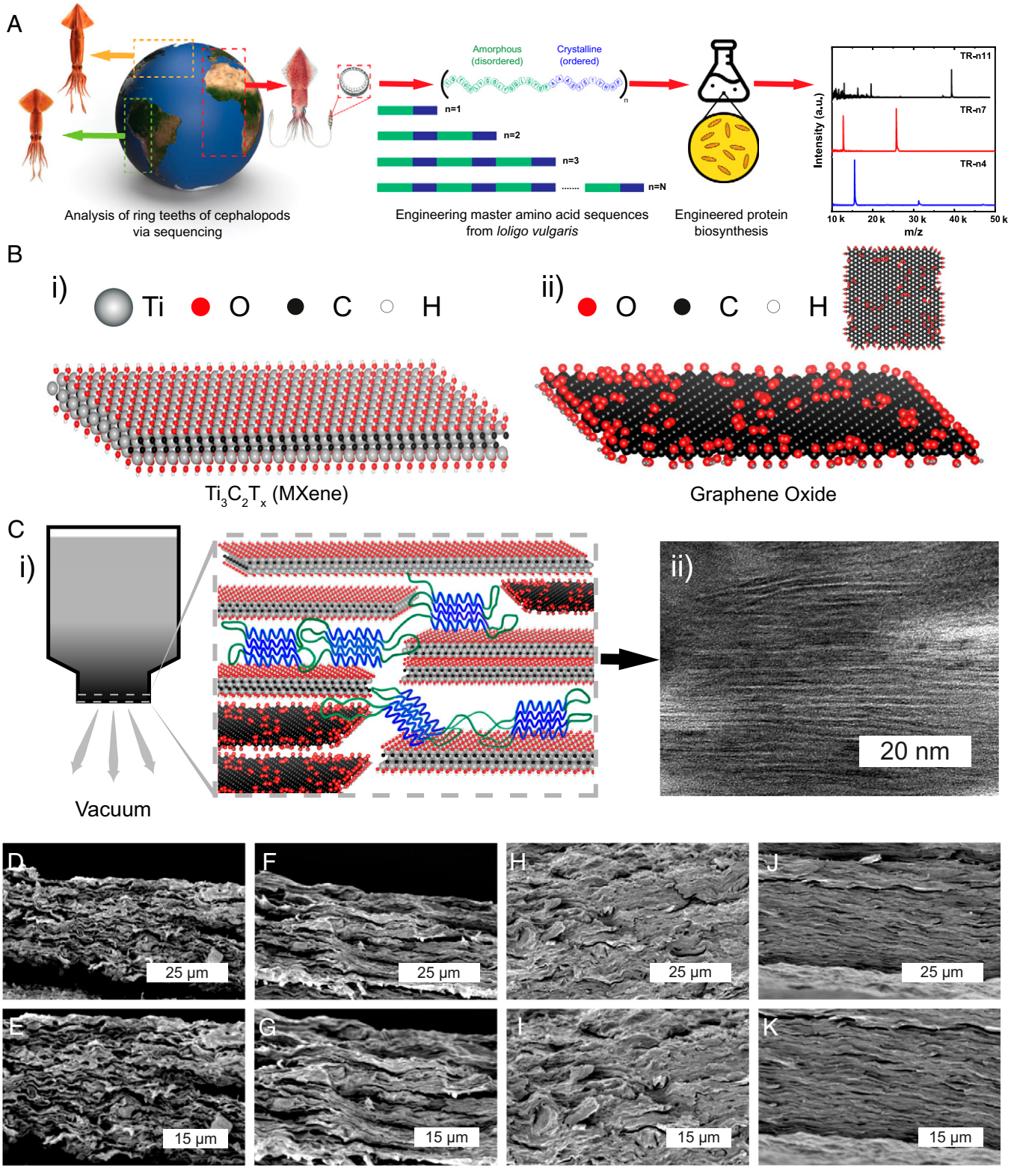

Fig. 2. (*A*) Schematic illustrations of tandem repeat protein design and corresponding matrix-assisted laser desorption ionization data for molecular weight analysis of TR proteins. (*B*) Schematic of 2D nanosheets for (*i*) MXene and (*ii*) graphene oxide, and (*C*) (*i*) fabrication process and ultimate structure of resulting tough composites along with a corresponding (*ii*) cross-section TEM image of MX/TR-n11 composites. SEM images acquired in low and high magnifications for (*D*, *E*) GO/MX composites, (*F*, *G*) GO/MX/TR-n4 composites, (*H*, *I*) GO/MX/TR-n7 composites, and (*J*, *K*) GO/MX/TR-n11 composites, respectively.

capability (3, 38). To orchestrate the structure and mechanical properties of the resultant composites, we introduced engineered proteins with three different sizes, which are determined by the number of repeat units (n, $n = 4$, $n = 7$, and $n = 11$ corresponding to molecular weight of 15 kDa, 25 kDa, and 40 kDa, respectively, according to matrix-assisted laser desorption ionization analysis) in the cumulative amino acid sequence (Fig. 2*A*). Freestanding bulk composites of GO, MXene, and TR proteins are prepared using vacuum-assisted self-assembly (VASA). 2D crystals of MXene (Fig. 2*B*, *i*) and GO (Fig. 2*B*, *ii*) are dispersed

and stabilized in dimethyl sulfoxide (DMSO) solutions as single or few-layer nanosheets. Relevant DMSO solutions of GO, MXene, and TR proteins are mixed and consequently filtered through a membrane to assemble into freestanding composites (Fig. 2*C*, *i*). We prepared composites that are composed of GO and TR proteins (GO/TR), MXene and TR proteins (MX/TR), and finally, GO, MXene, and TR proteins (GO/MX/TR) to investigate the influence of a secondary 2D crystal filler (Fig. 2*C*, *i* and *ii*).

To assess the organization of 2D crystals in GO/MX/TR composites, we performed cross-section scanning electron microscopy (SEM) analysis (Fig. 2*D*–*K*). The SEM images of GO/MX composites with the absence of TR proteins reveal a structure with multitude of voids and crystals organized in various directions (Fig. 2*D* and *E*). The images GO/MX/TR-n4 composites that are constructed by shortest TR proteins reflect a decrease in void frequency with the bridging influence of proteins, however, the organization of 2D crystals is still not compact enough, and randomness in their organization is still visible (Fig. 2*F* and *G*). The images of GO/MX/TR-n7 pictures a more compact structure that is nearly void-free, yet random orientation of 2D crystals is intact (Fig. 2*H* and *I*). SEM images of GO/MX/TR-n11 present the most compact and highly organized composite structure with 2D crystals aligned parallel to the surface (Fig. 2*J* and *K*).

Structural and Compositional Study of Bioengineered Composites

To unveil individual structural influence of GO, MXene crystals, and TR proteins in GO/MX/TR composites, we investigated the microstructure of GO/TR, MX/TR, and GO/MX/TR composites using wide-angle X-ray scattering (WAXS) analysis (Fig. 3*A*–*C*). This analysis is particularly important to calculate the interlayer distance of 2D sheets as a function of "n" in GO/MX/TR composites. The increasing number of tandem repeat units results in similar separation in between GO and MXene crystals in GO/TR and MX/TR composites, which are simply composed of a single filler material (Fig. 3*D* and *E* and *SI Appendix*, Fig. S1). In case of GO/MX/TR composites, proteins selectively organize MXene nanosheets, while separation in between GO crystals

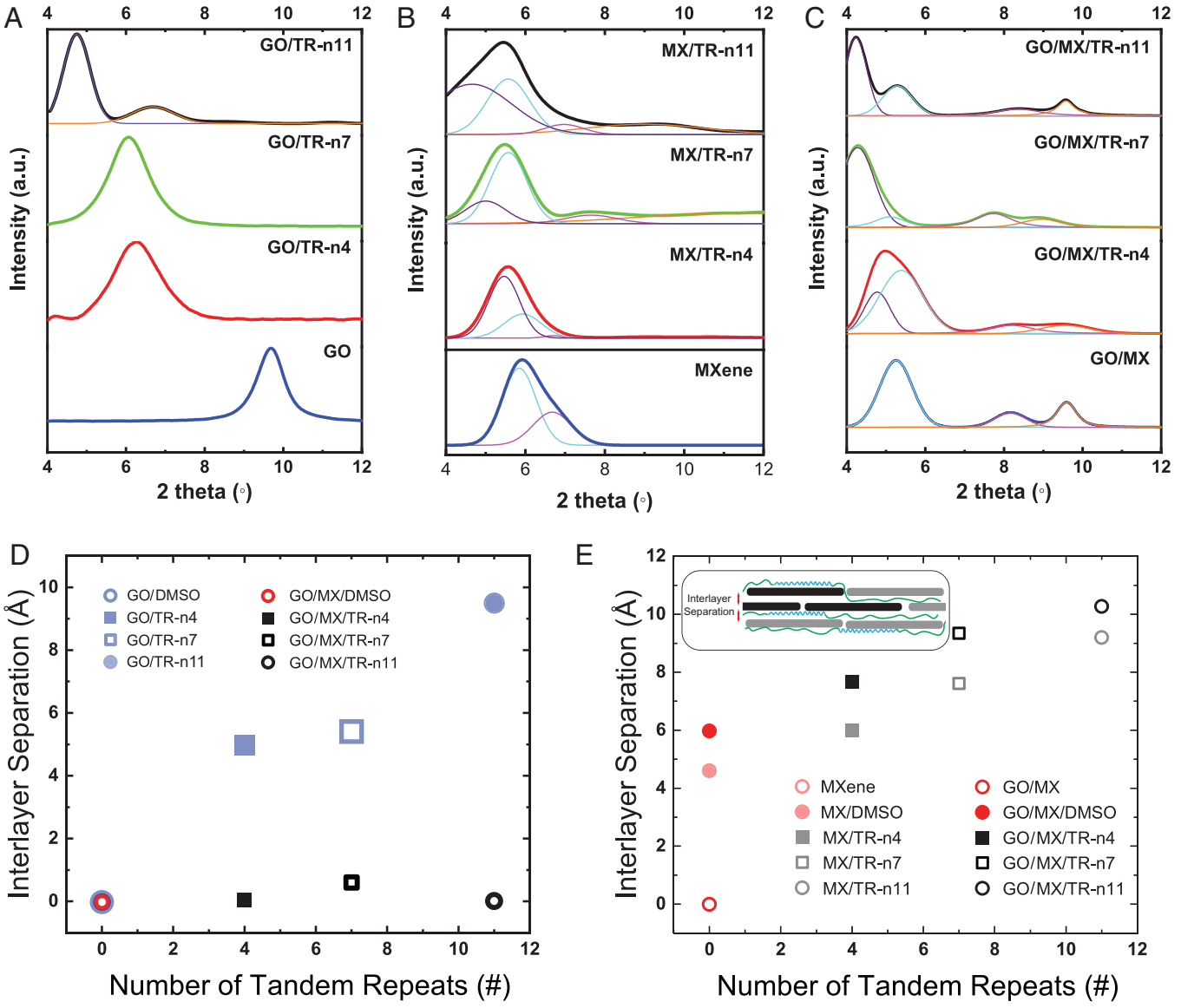

Fig. 3. Wide-angle X-ray diffraction (WAXS) data of (*A*) GO/TR composites, (*B*) MX/TR composites, and (*C*) GO/MX/TR composites. (*D*) Increase in interlayer separation (d-spacing) between GO nanosheets for GO/TR and GO/MX/TR composites. (*E*) Increase in interlayer separation (d-spacing) between MXene nanosheets for MX/TR and GO/MX/TR composites.

remains identical to pristine bulk GO paper (Fig. 3*D* and *E* and *SI Appendix*, Fig. S1). The WAXS data suggests that TR proteins having a higher number of tandem repeat units enhances the alignment of GO crystals in GO/TR composites (Fig. 3*A*). This can be inferred from the reduced full-width half maximum (FWHM) values of (002) diffraction peak of GO crystals in composites that consist of longer TR proteins (Fig. 3*A*). In contrast, TR proteins with lower number of tandem repeat units can organize MXene crystals much more efficiently, in comparison to MX/TR composites that composed of longer TR proteins (Fig. 3*B*). This is evidenced by the increasing FWHM values for (002) diffraction peak of MXene crystals once they are assembled by longer TR proteins in MX/TR composites (Fig. 3*B*). Similar to GO/TR composites, employing longer proteins with higher number repeat units introduces a more ordered 2D crystal distribution in GO/MX/TR composites (Fig. 3*C*). Both (002) peaks of MXene and GO crystals exhibit the lowest FWHM value in WAXS data of GO/MX/TR-n11 composites, which are composed of TR proteins with 11 repeat units (Fig. 3*C*). This observation is in line with the SEM analysis performed on GO/MX/TR composites, which indicates a more compact and ordered structure for composites with longer protein matrices (Fig. 2*D*–*K*). A similar structural influence is observed for structural nanocomposites that introduces a secondary nanosheet filler (24).

Structural characterization revealed that employing TR proteins with a different number of tandem repeats results in composites with systematically different interlayer separation and distinct order in the distribution of 2D crystals. However, to completely assess the impact of TR proteins on mechanical properties of GO/TR, MX/TR, and GO/MX/TR composites, it is essential to determine filler fraction of GO and MXene crystals in these materials. The composition of GO/TR, MX/TR, and GO/MX/TR composites are characterized using thermogravimetric analysis (TGA) to identify respective filler fractions. TGA data of GO/TR composite indicates an average GO filler weight fraction of 45 wt% and volume fraction of 38% (vol/vol) (Fig. 4*A* and *SI Appendix*, Table S1). Similar to GO/TR composites, MX/TR composites exhibit an average filler weight fraction of 45 wt%, yet it corresponds to a lower average volumetric filler fraction of 27% (vol/vol) (Fig. 4*B* and *SI Appendix*, Table S1). Evaluation of TGA data of GO/MX films and GO/MX/TR composites reveals that GO and MX have matching average weight filler fractions of 27.5 wt% in GO/MX films and GO/MX/TR composites (Fig. 4*C* and *SI Appendix*, Fig. S2). This corresponds to an average volume fraction of 26.5% (vol/vol) for GO and 15.5% (vol/vol) for MXene crystals (Fig. 4*C* and *SI Appendix*, Fig. S2 and Table S1). Fascinatingly, changes in number of tandem repeats for GO/TR, MX/TR, and GO/MX/TR composites have infinitesimally small impact on the composition of the composites (Fig. 4 and *SI Appendix*, Table S1). To summarize, this characterization suggests that these composites based on TR proteins exhibit similar filler fractions and a controllable diversity in their structure (Figs. 3 and 4). This behavior portrays a drastic contrast with respect to conventional composite systems, which relies on compositional differences to induce systematic changes in structure and mechanical properties of materials (15, 39). This structural and compositional peculiarity is particularly important for developing an understanding for the specific influence of the structure on mechanical properties excluding the impact of filler fraction. The TGA data also indicate the presence of trapped solvent molecules of water and DMSO, which can be identified from the peaks centered in the vicinity of 100 °C (water) and 190 °C (DMSO) at the derivatives of the TGA data (Fig. 4, *Insets*). The presence of certain solvent molecules are known to influence the structural confirmation of TR proteins (37), which can have serious implications on the mechanical properties of the GO/TR, MX/TR, and GO/MX/TR composites. In complement to TGA analysis, we performed a preliminary compositional characterization of secondary structures of proteins located in these composites with multiple fillers (GO/MX/TR composites) through infrared spectroscopy (*SI Appendix*, Fig. S3). Similar to GO/TR (38) and MX/TR[3], employing a TR protein with higher "n" leads to proteins with higher beta-sheet concentration (*SI Appendix*, Fig. S3*B*). This is supported by the structural characterization data as the gap between 2D nanosheets becomes larger with increasing "n", hence can accommodate formation of beta-sheets (Fig. 3*D* and *E*).

Mechanical Properties of Bioengineered Composites

The characterization of mechanical properties of GO/TR, MX/TR, and GO/MX/TR composites are performed through tensile stress-strain experiments (Fig. 5*A*–*E*). The presence of TR

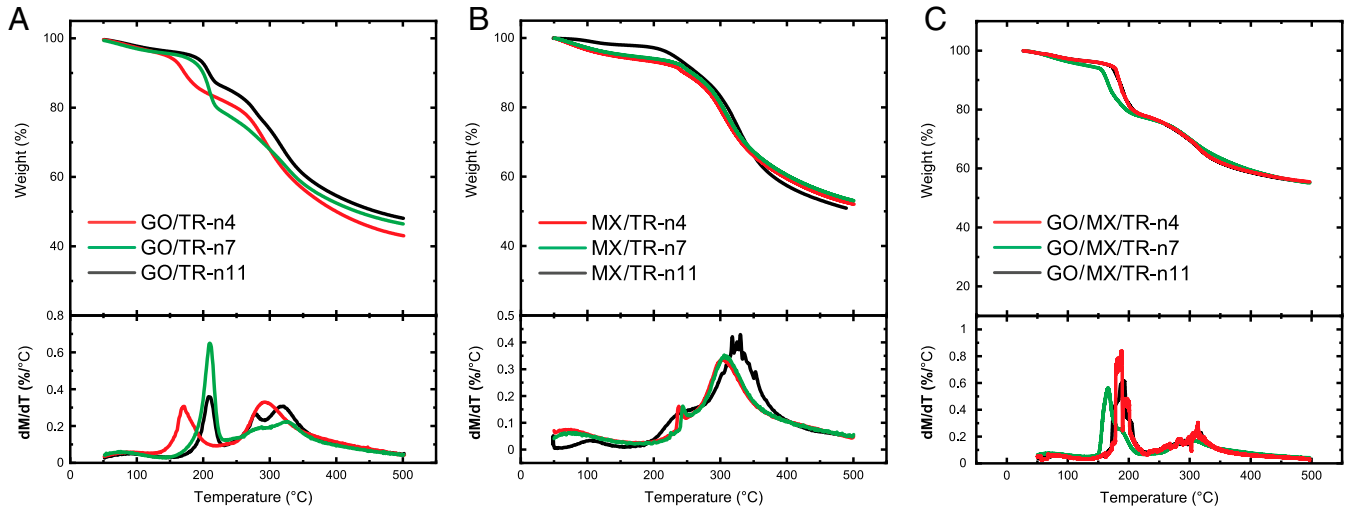

Fig. 4. Thermo-gravimetric analysis (TGA) data with wt% and derivative of wt% for (*A*) GO/TR composites, (*B*) MX/TR composites, and (*C*) GO/MX/TR composites.

proteins enhances ultimate tensile strength, fracture strain (elongation at break), and consequently toughness in GO/TR composites (Fig. 5*C*). Employing TR proteins with a higher number of tandem repeats results in stronger and tougher composites (Fig. 5*C*). Consequently, GO/TR-n11 composites can demonstrate tensile strength and elongation at break values of 175 ± 8 MPa and 16.6 ± 0.5% strain, respectively (Fig. 5*C* and *SI Appendix*, Table S2). In case of MX/TR composites, TR proteins help composites to maintain the ultimate tensile strength of freestanding MXene film, while drastically enhancing the fracture strain of the MX/TR composites (Fig. 5*D*). MX/TR-n11 composites can combine a tensile strength of 19 ± 0.3 MPa with an elongation at break value of 40 ± 0.5% strain (Fig. 5*D* and *SI Appendix*, Table S2 and Movie S1). The structural and compositional contributions of TR proteins to mechanical properties of composites manifest themselves strongest in GO/MX/TR composites (Fig. 5*E*). The incorporation of shortest ($n = 4$) TR proteins induces a trade-off in between ultimate tensile strength and fracture strain of GO/MX/TR composites (Fig. 5*E*). Increasing number of tandem repeats in GO/MX/TR composites leads to stronger and tougher composites, hence overcoming this trade-off for composites with "n" values reaching 7 (Fig. 5*E* and *F*). TR proteins contribute significantly to the fracture strain of GO/MX/TR composites. GO/MX/TR composites exhibit a drastic increase in elongation at break values with increasing "n" (Fig. 5*E* and *G*). This is not surprising, since earlier structural characterization suggested TR proteins selectively associate themselves with MXene crystals in GO/MX/TR composites (Fig. 3). Complementary to structural contributions from the assembly kinetics of MXene crystals and TR proteins, the presence of GO ensures a drastically stronger material system with tensile strength values exceeding 148 ± 2 MPa for GO/MX/TR composites (Fig. 5*E* and *F*). This composite system consisting of two distinct 2D crystal fillers and engineered proteins can have a mechanical compliance of 59 ± 1% strain under tensile deformation (Fig. 5*E* and *G*). Once these extraordinary mechanical aspects are combined in a composite material, it exhibits a toughness value of 54.8 ± 2 MJ/m^3 (Fig. 5*H*). This remarkable value exceeds state-of-the-art nacre-like composites engineered from 2D crystals (Fig. 5*I* and *J* and *SI Appendix*, Tables S2 and S3) (15–24, 30, 33, 34). Composites of graphene, graphene derivatives, and MXene crystals, as reported in the literature, commonly rely on drastic enhancements in ultimate tensile strength to achieve higher toughness in materials (15–20, 22, 23, 30). The recent introduction of a secondary 2D crystal filler that can interact with the primary 2D crystal filler and organic matrix in these composites has resulted in tougher materials (Fig. 5*J*) (24, 33). These hybrid composites can facilitate a more pronounced increase in fracture strain in exchange for a more moderate enhancement in tensile strength values (24, 33). However, GO/MX/TR-n11 composites with higher mechanical compliance and moderate ultimate tensile strength can reach toughness values that outrank these composites systems (Fig. 5*J*) (24, 33). This outline of mechanical properties suggests enhancing fracture strain of nacre-like composites without drastically compromising ultimate tensile strength could be an alternative approach for establishing mechanically tougher composites (Fig. 5*J*). More importantly, TR proteins offer the ability to alter fracture strain and toughness of composites systematically, which is not present for composite systems that employ drastic enhancements in tensile strength (Fig. 5*J*). To elucidate this aspect further, we presented scaling of ultimate tensile strength (Fig. 5*F*), elongation at break (Fig. 5*G*), and toughness (Fig. 5*H*) of GO/TR, MX/TR, and GO/MX/TR composites with respect to reciprocal number of tandem repeats (1/n). Reciprocal number of tandem repeats is a key parameter for unveiling the impact of molecular weight of TR proteins on their physical properties [e.g., not only mechanical (1) but also thermal (5, 38) and proton conductivity (40) as well as self-healing (4)]. The ultimate tensile strength of composites based on TR proteins does not show regular scaling with reciprocal number of tandem repeats (Fig. 5*F*). We propose that this scaling is disrupted by the formation of secondary structures in between 2D crystals in these composites (3, 38). The ultimate tensile strength of GO/TR composites increases moderately until number of tandem repeats reaching 11 that corresponds to reciprocal number of tandem repeats of 0.09. This "n" value corresponds to an interlayer distance between 2D crystals in GO/TR composites which is large enough to accommodate formation of beta-sheets (Fig. 3*D*) (3, 38). This onset "n" value for the formation of beta-sheets is 7 ($1/n = 0.14$) for both MX/TR and GO/MX/TR composites (Fig. 3*E*). Consequently, the ultimate tensile strength value of MX/TR-n7 and GO/MX/TR-n7 is drastically different from MX/TR-n4 and GO/MX/TR-n4 while these values are similar to ultimate tensile strength values of MX/TR-n11 and GO/MX/TR-n11 composites. In contrast, elongation at break values of TR-based composites exhibit an evident linear scaling with reciprocal number of tandem repeats, where each composite system presenting a different slope for scaling (Fig. 5*G*). GO/MX/TR composite systems demonstrate the most pronounced scaling, which is followed by MX/TR and GO/TR composite systems (Fig. 5*G*). In addition, each composite system with the lowest number of tandem repeats, hence the highest reciprocal number of tandem repeats, features similar elongation at break values (Fig. 5*G*). This highlights the consistent influence of templating capability of TR proteins on fracture strain of respective composites. In line with the scaling of elongation at break values of TR protein-based composites, toughness of these composites also presents a linear scaling with respect to reciprocal number of tandem repeats (Fig. 5*H*). Similar to scaling of elongation at break, scaling in toughness is most pronounced for GO/MX/TR composites, while composites with highest reciprocal number of tandem repeats converge into similar toughness values independent of their composition (Fig. 5*H*).

In Fig. 6, we show the theoretical estimations for mechanical properties of 2D composites consisting of heterostructured nanosheets with SRT proteins (e.g., GO/TR, MX/TR or GO/MX/TR). We performed a computational analysis of our composites consisting of nanosheet and protein layers using platelet-matrix theory (Movies S2 and S3). Our model involved interlayer distance of 2D crystals, d, their thickness, b, and width, L (Fig. 6*A*). A comprehensive understanding of the mechanics of platelet–matrix composites and stacked heterostructures in the shear mode via universal composition–structure–property maps was developed earlier (6, 31). Gao et al. (6) studied the impact fracture of natural composites (e.g., nacre and bone) where the soft protein phase plays a key role in alleviating impact damage to inorganic platelets. They demonstrated that the aspect ratio and the volume fraction of composites are inversely correlated to achieve the optimum stiffening of composites (i.e., in agreement with the Jaeger and Fratzl equation as shown in *SI Appendix*, Eq. S2). They concluded that the calcium-based platelets in human bone have much smaller size and larger aspect ratios in comparison with those found in seashells (as shown earlier in Fig. 1*A* and *B* respectively). This theoretical model guides our experimental design for obtaining required mechanical properties of our composites. Fig. 6*B* and *C* show stress-strain analysis from theoretical model as well as experimental values. It is possible to observe that this model can estimate the mechanical behavior of

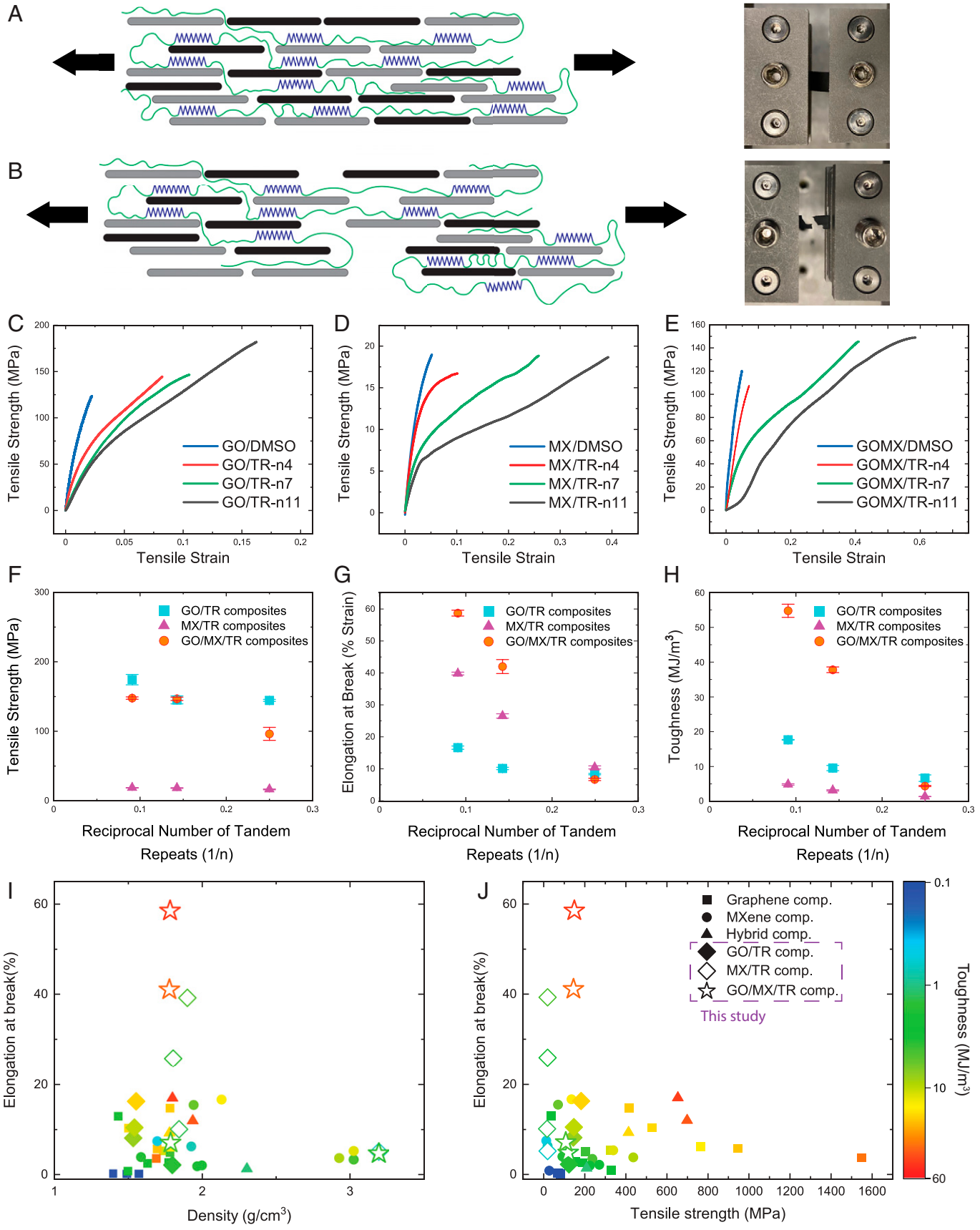

Fig. 5. Schematic illustration and images of 2D composites (*A*) before, and (*B*) after tensile deformation. Stress-strain data of (*C*) GO/TR, (*D*) MX/TR, and (*E*) GO/MX/TR composites. (*F*) Ultimate tensile strength, (*G*) elongation at break (fracture strain), and (*H*) toughness of GO/TR, MX/TR, and GO/MX/TR composites as a function of reciprocal number of tandem repeats (1/n) of respective protein matrices. (*I*) Comparative graph for evaluating elongation at break and toughness of GO/TR, MX/TR, GO/MX/TR, and existing composites of 2D materials as a function of density. (*J*) Comparative graph for evaluating elongation at break and toughness of GO/TR, MX/TR, GO/MX/TR, and existing composites of 2D materials as a function of ultimate tensile strength (the data set is provided in *SI Appendix*, Tables S2 and S3 in detail).

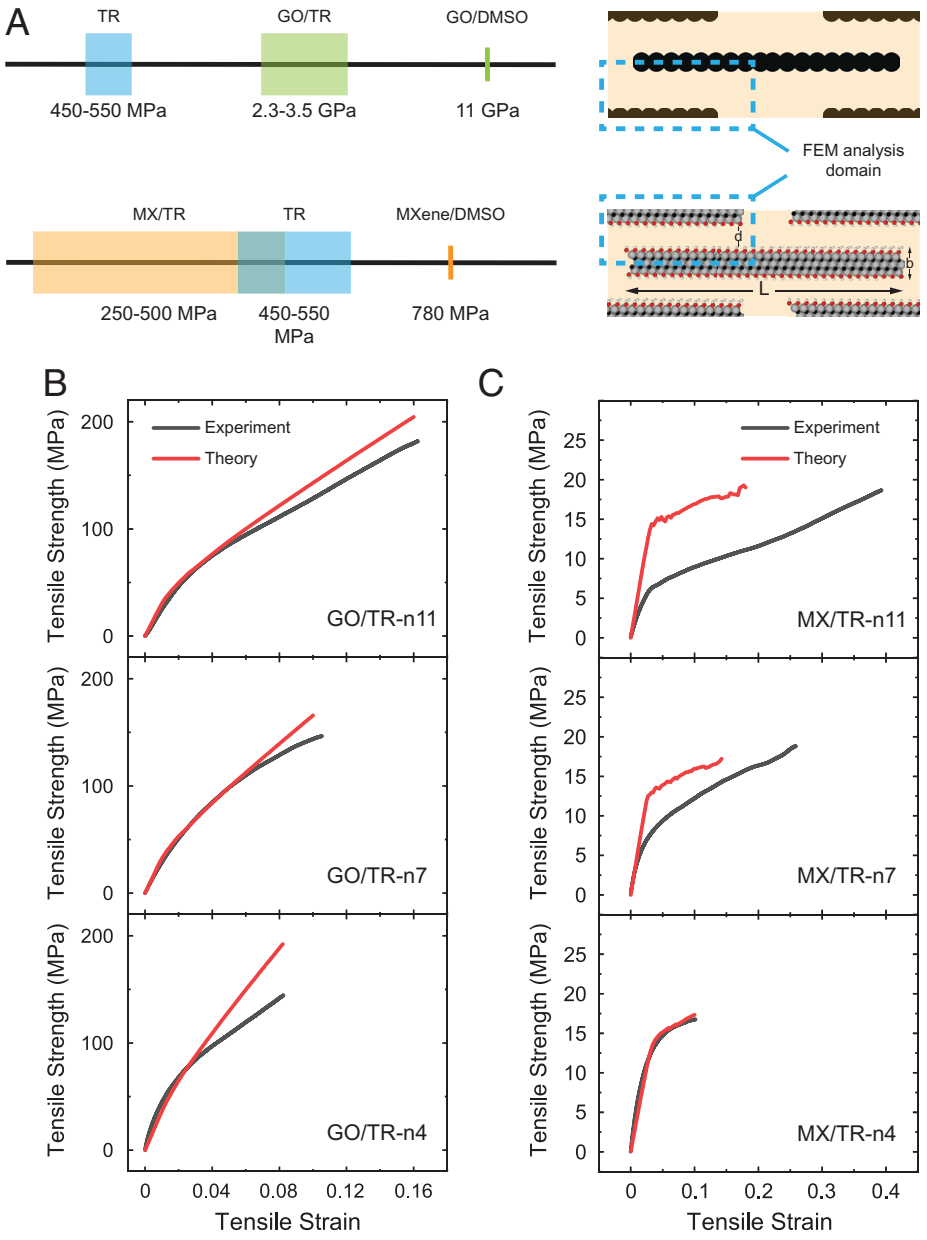

Fig. 6. (*A*) Schematic outline of mechanical properties of GO, MXene, and TR proteins and illustration of physical domain used in finite element analysis for GO/TR and MX/TR composites. Experimental and stress/strain curves compared with theoretical stress/strain curves of (*B*) GO/TR and (*C*) MX/TR composites estimated via finite element analysis.

GO/TR composites with different "n" values with considerable accuracy until "n" reaches 11 (Fig. 6*B*). The experimental stress–strain curve of GO/TR-n11 composite can deform exceeding 16% tensile strain, which agrees well with the computational model (Fig. 6*B*). However, computational analysis shows a deviation in between experimental and theoretical stress-strain curves of MX/TR composites with the onset "n" value of 7 (Fig. 6*C*). Experimental stress–strain curves of MX/TR-n7 and MX/TR-n11 exceed predicted fracture strain values by computational model (Fig. 6*C*), where the interface strength is weaker compared to GO fillers. These onset "n" values for GO/TR and MX/TR composites matches the onset "n" values for the formation of beta-sheets in between 2D nanosheets in these composites. To further elaborate, we previously identified that increasing "n" in TR proteins leads to materials with an extended range of plasticity (*SI Appendix*, Fig. S5) (1). This is originating from the enhanced ability to form beta-sheet crystals, which operate as anchors that help bridging more mobile segments of the proteins like amorphous sites and other secondary structures as demonstrated in our NMR studies (1, 37). Adding this information to our earlier observations regarding the ability of TR proteins to accommodate formation of beta-sheets in between 2D nanosheets, we can deduce that deviation from the model is due to the unique assembly kinetics in between TR proteins and 2D nanosheets. The assembly kinetics of these composites can facilitate formation of anchoring secondary structures at the interface of 2D nanosheets and enhance interfacial interactions in between TR proteins and 2D nanosheets (Fig. 6*A*). This is reflected on the ultimate mechanical properties including tensile strength and fracture strain (Figs. 5 and 6). Beyond tensile strength and fracture strain, stiffness of TR-based composites can be described using a simplified expression of E (Young's modulus as shown in *SI Appendix*, Eq. S1) (6). Therefore, low modulus of soft TR protein matrix can be compensated via the incredibly high aspect ratio of 2D nanosheets (i.e., 500–1,000). Hence, it is possible to accommodate higher protein concentrations, without significantly

compromising stiffness. In a geometry of alternating layers of 2D nanosheets and TR proteins with a dimension confined below 2 nm, these bioengineered composites with volumetric filler fractions limited below 40% can exhibit deformation mechanics of natural nacres with volumetric filler fractions remaining above 90% (6). Considering these structural dimensions are well below critical length scale described for layered nacre structures, these bioengineered composites are also impervious to flaws in their structure and can naturally accommodate more matrix material without compromising mechanical properties. To further elucidate, we provided theoretically estimated stiffness of layered composites of GO and MXene nanosheets with tandem repeat proteins and related experimental values (*SI Appendix*, Fig. S6). In the sum of these findings, we demonstrated the tunability of the strength, stiffness, and more importantly, plasticity of bioengineered composites by systematically altering the microstructure and composition (through formation of secondary structures at the interface of filler and matrix material) of layered nanocomposites.

Conclusion

In summary, we report a material system consisting of inorganic nanosheets and tandem repeat (TR) proteins as a nanoscale composite. Our work involved both experimental measurements and computational simulations to understand the uniaxial mechanical responses from composites of nanosheets (graphene oxide [GO] and layered titanium carbide [MXene]) with controllable interlayer distance. The key difference of these proteins from existing molecular templates used in composites can be stated as their ability to orchestrate a microstructure consisting of alternating layers of 2D nanosheets and proteins, which are confined into several nanometers. This structural impact allows these composites to mimic deformation kinetics of natural nacres making their mechanical properties impervious to structural flaws, while having a significantly lower filler fraction in comparison to nacre materials. The dimensions of separating protein layers can be controlled systematically using the length of proteins, which introduces a parameter alternative to filler fraction for engineering of mechanical properties in these composites. In complement to the structural influence of protein separation, these protein templates can also initiate compositional differences, once the spacing between 2D nanosheets is large enough to accommodate formation of beta-sheet crystals. These contributions are documented by experimental results and supported with the theoretical analysis of these composite systems. These tough materials, with additional functionality like electrical thermal conductivity, can find numerous applications as active materials in robotics and flexible and wearable electronics.

Materials and Methods

Synthesis of Tandem Repeat Proteins. Sequences of squid-inspired tandem repeat proteins are engineered using protein expression, gene sequencing, and protein design according to the protocol described earlier (1). Once the sequences are verified in plasmids, these are transferred to *Escherichia coli*. After colony inoculation and fermentation, cells are collected. Resultant product is processed to acquire purified tandem repeat proteins.

Synthesis of MXene. MXene is produced from MAX Phase (Ti_3AlC_2) precursor by a selective etching Al layer that separates titanium carbide nanosheets. This process involves preparation of an etching solution consisting of 6 M 20 mL HCl solution, which is placed into the Teflon round bottom flask. One gram of lithium fluoride and 1 g of unetched raw material is added gradually to the flask. This mixture is stirred at 60 °C for 24 h. To acquire etched material, the solution is centrifuged for 30 min at 6,000 rpm. The precipitate is washed with deionized water. This is repeated until pH is balanced at 6. Then, the water solvent is replaced with DMSO through solvent exchange. DMSO is an effective solvent for exfoliating MXene crystals into individual nanosheets. To ensure singe or few-layer sheets, these solutions are homogenized using mild tip sonication treatments for 30 min.

Synthesis of Graphene Oxide. As the initial step, 5 g of graphite flakes (<10 μm) and 25 g of potassium permanganate (oxidizer) is weighed out. Next, a solution of 200 mL sulfuric acid and 40 mL phosphoric acid is made and set to stir at 40 °C. The graphite is then added to the solution and allowed to stir until the flakes were uniformly suspended throughout the solution. Once the graphite flakes are uniformly dispersed in the solution, oxidizer is slowly added to the solution and allowed to stir at 500 RPM for 4 h. Then, the reaction is stopped and allowed to cool at room temperature. This solution is poured into a cold mixture (4 °C) of consisting of 600 mL of water and 40 mL of hydrogen peroxide; the peroxide neutralizes excess unreacted oxidizers remaining in the solution. The graphene oxide product is left to sediment, and then the solution is decanted so that only a graphene oxide cake remains at the bottom (yellow-brownish color). The sediment is then dispersed in a 1-L solution of 5% sulfuric acid. The 1-L acid solution is then centrifuged at 4,000 rpm for 3 min, and after the centrifugation, the solution is decanted. The resulting solution is washed with equal parts of deionized water, repeated three times. A final wash with a 1 mM acid solution (hydrochloric or sulfuric acid) is performed, and the resulting solution is centrifuged at 6,000 rpm for 3 h. Once the final product is achieved it is filtered and dried in a vacuum desiccator overnight.

Preparation of Composites. Batch solutions consisting of MXene and GO crystals that are dispersed in DMSO are employed to fabricate tough composites of tandem repeat proteins. For GO/TR composites, 30 mL GO-DMSO (with 1 mg/mL concentration) is gradually mixed with 20 mL TR protein-DMSO (with 7.5 mg/mL concentration) solution. This solution is filtered through a Anodisc membrane filter (diameter, 47 mm; pore size, 0.2 mm) with a vacuum flocculator. This is essential to facilitate slow assembly kinetics of vacuum assisted self-assembly (VASA). Similarly, MXene/TR composites are prepared through mixing 30 mL of MXene-DMSO (with 1 mg/mL concentration) and 20 mL TR protein-DMSO (with 7.5 mg/mL concentration) solution. These solutions are processed with VASA to result in free-standing tough composites. GO/MX/TR composites are prepared from a mixture solution that is composed of 15 mL GO-DMSO (with 1 mg/mL concentration), 15 mL MXene-DMSO (with 1 mg/mL concentration), and 20 mL TR protein-DMSO (with 7.5 mg/mL concentration) solution. This ternary mixture is processed with VASA as well to result in GO/MX/TR composites.

Characterization. SEM images are acquired using ZEISS 55 Ultra FESEM at 10 kV voltage. Wide angle X-ray scattering characterizations are performed via Malvern Panalytical Empyrean (third gen.) Nacre sample is commercially purchased (Trees of the Land). Composites samples are prepared using VASA method. X-ray diffractometer is equipped with microfocus and sealed copper tube under vacuum at room temperature. The measurement wavelength is 1.54 Å (50 kV, 0.6 mA). Thermogravimetric analysis (TGA) analysis is performed using TA Instruments SDT Q600 with alumina pots and under nitrogen environment ($n = 3$, error bars represent SD). Tensile deformation measurements are performed using the mechanical stage from Psylotech Inc. For these measurements, a 100 N load cell is employed ($n = 3$, error bars represent SD). Composites in rectangular shape (4 mm × 2 mm) underwent tensile deformation with a constant loading rate of 5 μm/s. These measurements are performed under room temperature and ambient humidity conditions.

Computational Model. The commercial finite element analysis software Abaqus (Dassault Systèmes) was used to conduct simulations for the numerical examples in this work (see *SI Appendix*, Table S4 for complete set of parameters). The simulated structure was selected as the quarter of a tension-shear-chain unit cell, which contains two platelet quarters and connecting matrix between them (as shown in Fig. 6*A*, and Movies S1–S3). The aspect ratio is 0.118 for both GO and MXene nanoplatelets, and the aspect ratio of the whole unit cell is 0.457. The volumetric filler fractions of 2D materials were kept the same as the measured values in experiment. Linear elastic materials were used to model the 2D material nanoplatelets with the Young's modulus of 11.07 GPa for GO and 0.78 GPa for MXene. The protein matrix was modeled as elastic-plastic material with the measured

constitutive law data reported earlier (1). The cohesive traction-separation behavior was used to model the interfacial interaction between 2D nanoplatelets and protein matrix. Prescribed displacement was exerted on one lateral side of the unit cell, and symmetric boundary conditions were applied to the other sides. Four-node bilinear quadrilateral solid elements (CPE4R) with reduced integration were adopted to mesh the platelets and matrix.

Data Availability. All data inthis study are included in the article and/or *SI Appendix*.

ACKNOWLEDGMENTS. The authors thank Penn State's Materials Research Institute and Huck Life Science Institute staff members for helpful discussions. We also thank Robert Neuweiler and Burcu Dursun for graphene oxide synthesis and recording composite movie respectively. M.V., T.M., O.C., and M.C.D. were partially supported by DARPA (D19AC00016), Airforce Office of Sponsored Research (FA9550-18-1-0235), Army Research Office (W911NF-16-1-0019), and Huck Endowment of Pennsylvania State University. The views, opinions and/or findings expressed are those of the author and should not be interpreted as representing the official views or policies of the Department of Defense or the US government. D.L. and H.G. acknowledge a research start-up grant (002479-00001) from Nanyang Technological University and the Agency for Science, Technology and Research (A*STAR) and the use of the A*STAR Computational Resource Centre, Singapore (ACRC) and National Supercomputing Centre, Singapore (NSCC).

Author affiliations: [a]Center for Research on Advanced Fiber Technologies (CRAFT), Department of Engineering Science and Mechanics, Materials Research Institute, Pennsylvania State University, University Park, PA 16802; [b]College of Engineering and Science, Nanyang Technological University, 639798, Singapore; [c]College of Engineering, Brown University, Providence, RI, 02912; and [d]Huck Institutes of Life Sciences, Pennsylvania State University, University Park, PA 16802

1. H. Jung *et al.*, Molecular tandem repeat strategy for elucidating mechanical properties of high-strength proteins. *Proc. Natl. Acad. Sci. U.S.A.* **113**, 6478–6483 (2016).
2. H. Yilmaz *et al.*, Structural protein-based flexible whispering gallery mode resonators. *ACS Photonics* **4**, 2179–2186 (2017).
3. M. Vural *et al.*, Self-assembly of topologically networked protein-Ti_3C_2Tx MXene composites. *ACS Nano* **14**, 6956–6967 (2020).
4. A. Pena-Francesch, H. Jung, M. C. Demirel, M. Sitti, Biosynthetic self-healing materials for soft machines. *Nat. Mater.* **19**, 1230–1235 (2020).
5. J. A. Tomko *et al.*, Tunable thermal transport and reversible thermal conductivity switching in topologically networked bio-inspired materials. *Nat. Nanotechnol.* **13**, 959–964 (2018).
6. H. Gao, B. Ji, I. L. Jäger, E. Arzt, P. Fratzl, Materials become insensitive to flaws at nanoscale: Lessons from nature. *Proc. Natl. Acad. Sci. U.S.A.* **100**, 5597–5600 (2003).
7. U. G. K. Wegst, H. Bai, E. Saiz, A. P. Tomsia, R. O. Ritchie, Bioinspired structural materials. *Nat. Mater.* **14**, 23–36 (2015).
8. F. Barthelat, H. Tang, P. D. Zavattieri, C.-M. Li, H. D. Espinosa, On the mechanics of mother-of-pearl: A key feature in the material hierarchical structure. *J. Mech. Phys. Solids* **55**, 306–337 (2007).
9. R. Z. Wang, Z. Suo, A. G. Evans, N. Yao, I. A. Aksay, Deformation mechanisms in nacre. *J. Mater. Res.* **16**, 2485–2493 (2001).
10. P. Fratzl, H. S. Gupta, E. P. Paschalis, P. Roschger, Structure and mechanical quality of the collagen–mineral nano-composite in bone. *J. Mater. Chem.* **14**, 2115–2123 (2004).
11. E. A. McNally, H. P. Schwarcz, G. A. Botton, A. L. Arsenault, A model for the ultrastructure of bone based on electron microscopy of ion-milled sections. *PLoS One* **7**, e29258 (2012).
12. S. Li, E. Demirci, V. V. Silberschmidt, Variability and anisotropy of mechanical behavior of cortical bone in tension an2d compression. *J. Mech. Behav. Biomed. Mater.* **21**, 109–120 (2013).
13. Z. Tang, N. A. Kotov, S. Magonov, B. Ozturk, Nanostructured artificial nacre. *Nat. Mater.* **2**, 413–418 (2003).
14. J. Wang, Q. Cheng, L. Lin, L. Jiang, Synergistic toughening of bioinspired poly(vinyl alcohol)-clay-nanofibrillar cellulose artificial nacre. *ACS Nano* **8**, 2739–2745 (2014).
15. K. W. Putz, O. C. Compton, M. J. Palmeri, S. B. T. Nguyen, L. C. Brinson, High-nanofiller-content graphene oxide-polymer nanocomposites via vacuum-assisted self-assembly. *Adv. Funct. Mater.* **20**, 3322–3329 (2010).
16. Y.-Q. Li, T. Yu, T.-Y. Yang, L.-X. Zheng, K. Liao, Bio-inspired nacre-like composite films based on graphene with superior mechanical, electrical, and biocompatible properties. *Adv. Mater.* **24**, 3426–3431 (2012).
17. K. Hu, M. K. Gupta, D. D. Kulkarni, V. V. Tsukruk, Ultra-robust graphene oxide-silk fibroin nanocomposite membranes. *Adv. Mater.* **25**, 2301–2307 (2013).
18. W. Cui *et al.*, A strong integrated strength and toughness artificial nacre based on dopamine cross-linked graphene oxide. *ACS Nano* **8**, 9511–9517 (2014).
19. Z. Ling *et al.*, Flexible and conductive MXene films and nanocomposites with high capacitance. *Proc. Natl. Acad. Sci. U.S.A.* **111**, 16676–16681 (2014).
20. S. Wan *et al.*, Use of synergistic interactions to fabricate strong, tough, and conductive artificial nacre based on graphene oxide and chitosan. *ACS Nano* **9**, 9830–9836 (2015).
21. L. Zong, M. Li, C. Li, Bioinspired coupling of inorganic layered nanomaterials with marine polysaccharides for efficient aqueous exfoliation and smart actuating hybrids. *Adv. Mater.* **29**, 1604691 (2017).
22. S. Wan *et al.*, Sequentially bridged graphene sheets with high strength, toughness, and electrical conductivity. *Proc. Natl. Acad. Sci. U.S.A.* **115**, 5359–5364 (2018).
23. S. Wan *et al.*, Strong sequentially bridged MXene sheets. *Proc. Natl. Acad. Sci. U.S.A.* **117**, 27154–27161 (2020).
24. T. Zhou *et al.*, Ultratough graphene–black phosphorus films. *Proc. Natl. Acad. Sci. U.S.A.* **117**, 8727–8735 (2020).
25. K. S. Novoselov *et al.*, Two-dimensional atomic crystals. *Proc. Natl. Acad. Sci. U.S.A.* **102**, 10451–10453 (2005).
26. A. K. K. Geim, K. S. S. Novoselov, The rise of graphene. *Nat. Mater.* **6**, 183–191 (2007).
27. K. F. Mak, C. Lee, J. Hone, J. Shan, T. F. Heinz, Atomically thin MoS_2: a new direct-gap semiconductor. *Phys. Rev. Lett.* **105**, 136805 (2010).
28. M. Naguib *et al.*, Two-dimensional nanocrystals produced by exfoliation of Ti_3AlC_2. *Adv. Mater.* **23**, 4248–4253 (2011).
29. L. Mao *et al.*, Stiffening of graphene oxide films by soft porous sheets. *Nat. Commun.* **10**, 3677 (2019).
30. S. Wan *et al.*, High-strength scalable graphene sheets by freezing stretch-induced alignment. *Nat. Mater.* **20**, 624–631 (2021).
31. N. Sakhavand, R. Shahsavari, Universal composition-structure-property maps for natural and biomimetic platelet-matrix composites and stacked heterostructures. *Nat. Commun.* **6**, 6523 (2015).
32. S. Wan, L. Jiang, Q. Cheng, Design principles of high-performance graphene films: interfaces and alignment. *Matter* **3**, 696–707 (2020).
33. S. Wan *et al.*, Fatigue resistant bioinspired composite from synergistic two-dimensional nanocomponents. *ACS Nano* **11**, 7074–7083 (2017).
34. U. Khan, P. May, A. O'Neill, J. N. Coleman, Development of stiff, strong, yet tough composites by the addition of solvent exfoliated graphene to polyurethane. *Carbon* **48**, 4035–4041 (2010).
35. S. J. Kim, K. Choi, B. Lee, Y. Kim, B. H. Hong, Materials for flexible, stretchable electronics: Graphene and 2D materials. *Annu. Rev. Mater. Res.* **45**, 63–84 (2015).
36. H. Jang *et al.*, Graphene-based flexible and stretchable electronics. *Adv. Mater.* **28**, 4184–4202 (2016).
37. R. C. A. Dubini, H. Jung, C. H. Skidmore, M. C. Demirel, P. Rovó, Hydration-induced structural transitions in biomimetic tandem repeat proteins. *J. Phys. Chem. B* **125**, 2134–2145 (2021).
38. M. Vural *et al.*, Programmable molecular composites of tandem proteins with graphene oxide for efficient bimorph actuators. *Carbon* **118**, 404–412 (2017).
39. P. Samorì, I. A. Kinloch, X. Feng, V. Palermo, Graphene-based nanocomposites for structural and functional applications: Using 2-dimensional materials in a 3-dimensional world. *2D Mater.* **2**, 030205 (2015).
40. A. Pena-Francesch *et al.*, Programmable proton conduction in stretchable and self-healing proteins. *Chem. Mater.* **30**, 898–905 (2018).